— 2 —

Photons — from source to detector

Klaus Wilhelm[I] and Claus Fröhlich[II]

Abstract

The central theme of the book "Observing Photons in Space" is the detection and characterization of photons with instruments aboard spacecraft. This chapter presents a global overview of the fundamental processes that accompany photons all the way from their origin in the source region to their detection in our instruments. The radiation of the Sun is taken as example in some cases and is treated in more detail.

Introduction

The goal of observing photons clearly is to learn something about the regions that are emitting the radiation, and it is, therefore, necessary to understand the basics of the interaction of photons with matter at the source, during transit, and at the detection site. The last point is the most important one in the context of this book, but some generation and transfer processes have to be mentioned as well. Many of these aspects are discussed in more detail elsewhere in this book and cross-references are provided.

The interaction of photons with matter is mainly governed by two equations derived by Einstein (1905a,c). They can be written in a modern format as

$$E_\nu = h\,\overline{\nu} = h\,c_0/\overline{\lambda} \quad \text{and} \quad E_0 = m\,c_0^2\,, \tag{2.1}$$

where $h = 6.626\,068\,57(29) \times 10^{-34}$ J s is the Planck constant[1], E_ν is the energy quantum of electromagnetic radiation with mean values[2] of the frequency $\overline{\nu}$ and wavelength $\overline{\lambda}$, and $c_0 = \nu\,\lambda = 299\,792\,458$ m s^{-1} (exact) is the speed of light in

[I]MPS—Max-Planck-Institut für Sonnensystemforschung, Katlenburg-Lindau, Germany.
[II]PMOD / WRC—Physikalisch-Meteorologisches Observatorium Davos/World Radiation Center, Davos, Switzerland.

[1]This and other constants are taken from "CODATA recommended values of the fundamental physical constants: 2006" (Mohr et al 2008), or when available from 2010 CODATA at http://physics.nist.gov/cuu/constants.

[2]In the following discussion, the notations ν and λ will be used to simplify the equations, unless emphasis is placed on the fact that mean values are considered in special cases.

M.C.E. Huber et al. (eds.), *Observing Photons in Space: A Guide to Experimental Space Astronomy*, ISSI Scientific Report Series 9, DOI 10.1007/978-1-4614-7804-1_2,

vacuum[3]. E_0 is the rest energy of the mass m. The energy and momentum of a free massive particle moving with a velocity $\boldsymbol{v}$ relative to a reference frame S can be obtained from

$$E^2 - \boldsymbol{p}^2\, c_0^2 = m^2\, c_0^4 \tag{2.2}$$

and

$$\boldsymbol{p} = \boldsymbol{v}\, \frac{E}{c_0^2}\ , \tag{2.3}$$

where E is the total energy, $\boldsymbol{p}$ the momentum, and m the ordinary mass, the same as in Newtonian mechanics (Okun 1989). With $\beta = v/c_0$ ($v = |\boldsymbol{v}| < c_0$) and $\gamma = (1-\beta^2)^{-1/2} \geq 1$, the Lorentz factor, it is

$$E = \gamma\, m\, c_0^2\ . \tag{2.4}$$

The mass is zero for photons[4] and Equation 2.2 reduces in a region with a gravitational potential $\phi = 0$ (see page 29) to

$$E_\nu = p_\nu\, c_0\ . \tag{2.5}$$

It must, however, be emphasized from the outset that the wave theory of electromagnetic radiation as formulated by Young, Huygens, Fresnel, Maxwell and Hertz is a valid description of most of the observations as long as the energy quantization in Equation 2.1 is of no importance (see, e.g., Born and Wolf 1999; Jackson 1999). Consequently, the laws of physical optics, and even of geometrical optics are relevant to a large extent; in particular, those concerning the propagation of radiation. This permits the use of ray-tracing procedures. In the following, the wave or particle aspects of electromagnetic radiation will, therefore, be emphasized as required. The wave theory is also adequately describing the polarization properties of radiation (treated in detail in Chapters 33 to 35, Stenflo 2013; Hajdas and Suarez-Garcia 2013; Carretti and Rosset 2013), which correspond to the spin $s = 1$ of photons. Major modifications are, however, required during photon emission and absorption processes. The quantum electrodynamics developed by Born et al (1926), Dirac (1927), and others include most of these modifications, and renders a suitable description of photons (cf., e.g., Glauber 2007), albeit their "existence" is not generally accepted (Lamb 1995).

Special mention must be made of entangled states of photons as an important quantum physical phenomenon, although no application in astrophysical observations is known at this stage, other than the two-photon emission in the hydrogen spectrum detected by Brugel et al (1982). In response to the *Gedankenexperiment* of Einstein et al (1935) stipulating that entangled particles no longer interact after their separation, an inequality was formulated by Bell (1964) that would be valid under this condition. Since then, many violations of Bell's inequality, in the formulation of Clauser et al (1969), have been observed. One of the most recent tests was

[3] Follows from the definition of the SI base unit "metre" (BIPM 2006).

[4] A zero mass follows from the special theory of relativity and a speed of light in vacuum constant for all frequencies. Various methods have been used to constrain the photon mass to $m_\nu < 10^{-49}$ kg (cf., Amsler et al 2008, Goldhaber and Nieto 1971). These authors also discuss the consequences of a finite mass for the existence of longitudinal electromagnetic waves.

performed over a distance of more than 10 km yielding a speed for the quantum influence of at least $1 \times 10^3\, c_0$ (Zbinden et al 2001). The remaining critique of such experiments is that statistical results obtained by observing ensembles of photons are applied to a single photon pair; thus, it is claimed, it would still be possible to accept the physical reality of a photon (cf., Tiwari 2002; Adenier 2008).

In this context, experiments are of interest that study the structure of photons (Nisius 2000), and those demonstrating that two-photon interference cannot always be understood as the effects of two single photons (Strekalov et al 1998). It is worth noting that bunching of two photons in a symmetric state has been observed as a consequence of their bosonic nature by Hong et al (1987). Concerning the latter behaviour of photons see also Bose (1924) and Ehrenfest (1925).

Some photon generation processes

The most fundamental source of radiation is a so-called "black body", a system that absorbs all radiation impinging on it, i.e., the absorption coefficient is $\alpha_\lambda = 1$ for all λ. Kirchhoff's law then yields the emission coefficient $\epsilon_\lambda = 1$ at all wavelengths. The absorption coefficient $\alpha_\lambda = 1$ obviously means that a black body, or a representation of it, is a good detector for total irradiance measurements. Depending on its temperature, T, such a system emits radiation according to Planck's law[5] (Planck 1900, 1901) derived from a quantization of the radiation field

$$L_\lambda(T) = \frac{2\,h\,c_0^2}{\lambda^5}\left[\exp\left(\frac{h\,c_0}{\lambda\,k_\mathrm{B}T}\right) - 1\right]^{-1} \quad , \tag{2.6}$$

where $k_\mathrm{B} = 1.380\,6504(24) \times 10^{-23}\ \mathrm{J\,K^{-1}}$ is the Boltzmann constant and $L_\lambda(T)$ the spectral radiance at the wavelength λ. The corresponding formula for $L_\nu(T)$ is

$$L_\nu(T) = \frac{2\,h\,\nu^3}{c_0^2}\left[\exp\left(\frac{h\,\nu}{k_\mathrm{B}T}\right) - 1\right]^{-1} \quad . \tag{2.7}$$

The Cosmic Microwave Background (CMB) at $T_\mathrm{CMB} = 2.726$ K (Penzias and Wilson 1965; Mather et al 1990, 1994) is an example of black-body radiation (cf., Chapter 8, Lamarre and Dole 2013). It is thought to have been released from the "Big Bang plasma", when it changed from the optically thick to thin state at the time of atom formation (Dicke et al 1965). The CMB is probably the earliest electromagnetic radiation released after the Big Bang that is still accessible to us. Since the temperature at the time of atom formation was typically 3000 K, a redshift of z between $\approx$1000 and 1500 (Sunyaev and Zel'dovich 1980) has to be assumed.

A black body is the extreme case of an optically thick medium. In the Universe, many plasma systems emit radiation approximately according to Equation 2.6, at least, in certain wavelength ranges, for which a brightness temperature, T_B, can then be defined in local thermal equilibrium. Other regimes, although still optically thick, deviate from such an equilibrium and require radiation transfer calculations.

[5] Einstein and Stern (1913) argued in favour of a zero-point energy $h\,\nu/2$ of a resonator, first introduced by Planck (1909). The zero-point energy of the electromagnetic field causes, for instance, the Casimir forces (cf., Casimir 1949; Mohideen and Roy 1998).

Regions that are optically thin for some or all wavelengths represent the other extreme, and allow the integration of the radiation along the line of sight (LOS).

Many photon emissions are a consequence of electron transitions in atomic species from a higher energy level, E_2, to a lower one, E_1, as postulated by Bohr in 1913:

$$\overline{E_2} - \overline{E_1} = h\,\overline{\nu_{21}} \quad , \tag{2.8}$$

with $\overline{E_2}, \overline{E_1}$ the levels of the unperturbed states; an assumption that has to be modified in the light of Equation 2.9. The recoil of the emitter leads to an additional frequency shift depending on the details of the process.

In general, these emissions are spontaneous, but can also be stimulated by appropriate photon fluxes (Einstein 1917) — a prerequisite of any laser operation. Equation 2.8 also describes photon absorption if $E_2 < E_1$. The latter process can be considered as an excitation mechanism of molecules, atoms or ions, and will be of importance for the detection of photons. Excitations can also be induced by collisions between atomic species and electrons. Whenever inner electrons of an atom were involved in such transitions, the emitted radiation was historically called Röntgenstrahlung or X-rays. If the radiation was generated by transitions of excited nuclei of atoms, it was called gamma-rays. However, in modern terms X-ray and gamma-ray radiations are defined by their photon energies.

Additional generation processes of radiation involve accelerated or decelerated particles, in particular electrons, such as synchrotron radiation and bremsstrahlung. The annihilation of matter and antimatter should also be mentioned. In the case of an electron and a positron, the process produces, in general, two gamma-ray photons of 511 keV energy, each. A prominent gamma-ray line at 2.223 MeV is caused by neutron capture of hydrogen. Details on the thermal and non-thermal radiation of high-energy particles are discussed in Chapters 3 and 4 (Kanbach et al 2013; Culhane 2013). A special case is the $\lambda = 21.106$ cm line generated in the Universe by an electron spin reversal with respect to the proton spin in hydrogen atoms. Rotational transitions in molecular clouds are another source of low-energy photons.

The generated electromagnetic radiation is, as we have seen, released and absorbed as photons, quantized in energy. Einstein (1917) showed that the generation of a photon as a spherical wave is not possible, because a momentum transfer is invariably involved in the emission process. Given a certain atomic transition, the released energy is generally rather well defined resulting in a nearly mono-energetic photon flux, or, in the equivalent description, in waves with a frequency, ν_0, and wavelength, λ_0. Consequently, such a transition can be identified by the detection of a spectral line at λ_0. Atoms, ions and molecules emit a multitude of spectral lines related to their energy levels. Even a summary of the physics of these transitions would be far beyond the scope of this chapter. It suffices to say that the lines allow us to deduce elemental abundances, ionization stages, densities, electron and ion temperatures, and other parameters of the source regions. Selected spectra of the Sun might serve as example here:

Figure 2.1 depicts the vacuum-ultraviolet (VUV) radiance spectrum of a quiet-Sun region with many emission lines and some continua in the wavelength range from 80 nm to 150 nm. At longer wavelengths, the emission lines fade out and absorption features — the Fraunhofer lines — become prominent as a consequence

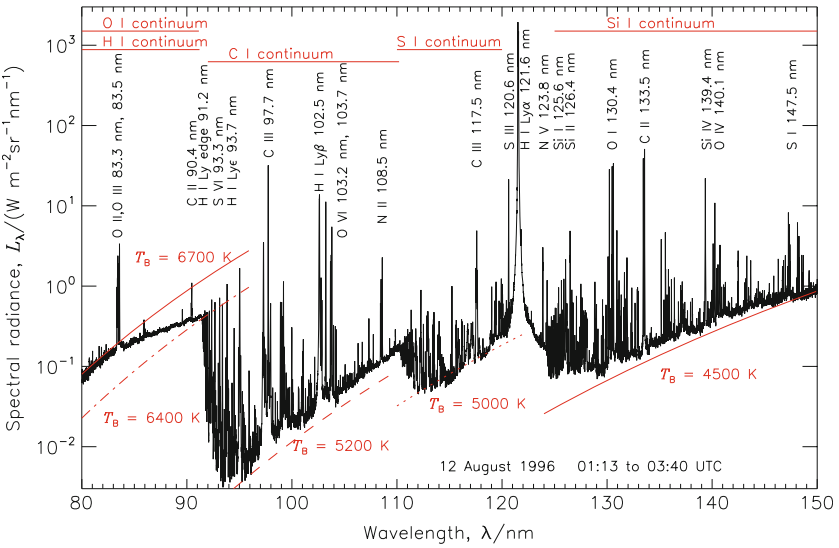

Figure 2.1: Spectral radiance of the quiet Sun in the VUV range from a region near the centre of the disk. Prominent emission lines are marked. The spectral radiances expected for some brightness temperatures, T_B, are shown in red as approximations of the continua in the corresponding wavelength ranges (after Wilhelm et al 2002).

of the thermal structure of the solar atmosphere. This can be seen in Figure 2.2 showing an irradiance spectrum of the Sun (Thuillier et al 2004). In general, these measurements are performed from platforms moving with respect to the source (the Sun). The necessary corrections are treated on page 36. Such spectra provide important information about the composition and other properties of the Sun or a star (see, e.g., Fröhlich et al 1998). Although the lines in Figures 2.1 and 2.2 appear to be rather narrow, they can be resolved into profiles by modern spectrometers furnishing information on motions in the solar atmosphere via the Doppler effect (cf., page 30). Similar measurements can be obtained from stellar and other cosmic objects. The spectrum of α Cen A, for instance, a G2 V star, closely resembles that of the Sun in the same spectral class (Ayres 2000).

Some emission lines are much wider than most of the other spectral profiles, in particular those from transitions of auto-ionization states, where the very short life times lead to a significant energy spread and a corresponding broadening (Avrett et al 2006). This is related to Heisenberg's uncertainty principle (Heisenberg 1927)

$$\Delta E \, t_H \geq \hbar \quad , \tag{2.9}$$

where t_H is the inner time of the decaying system (Aharonov and Bohm 1961), and is consistent with the derivation of Mandelstam and Tamm (1945) who defined t_H as the life time of a state with respect to a certain observable (cf., also Hilgevoord 1996, 1998).

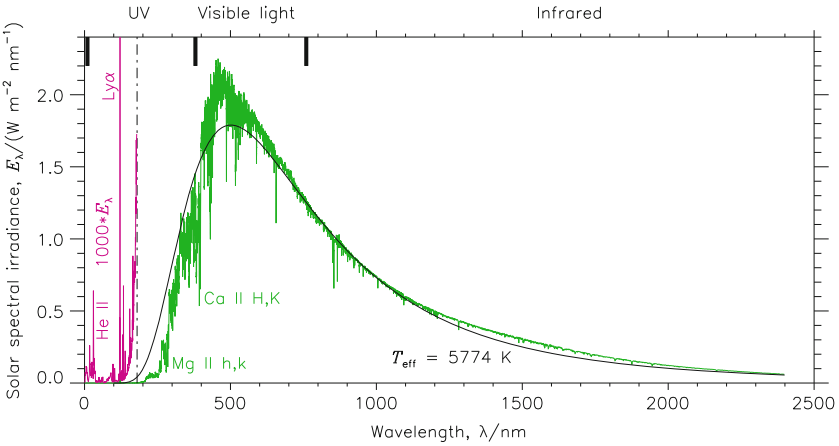

Figure 2.2: SSI, E_λ, of the quiet Sun at 1 ua (Data: Courtesy of G. Thuillier). For wavelengths below $\lambda = 180$ nm, 1000 E_λ is plotted in violet to show the low irradiance values in this range. The H I Lyα line is off the scale (cf., Figure 2.1). The ranges of the UV, visible and infrared radiations are marked on the top, and some prominent emission and absorption lines are indicated (cf., Chapters 5 to 7). The black curve shows the radiation of the Sun as a "black body" with $T_{\rm eff} = 5774$ K and a radius $R_\odot = 696.35$ Mm. The Sun also emits soft and hard X-rays as well as gamma-rays and radio waves, but the contributions to the total solar irradiance (TSI) are very small and highly variable (cf., Figure 2.3).

The solar spectral irradiance (SSI) in the visible wavelength region can be reliably determined from a high-altitude station. This was, for instance, done in the pioneering work of Labs and Neckel (1962, 1967) from the Jungfraujoch in the Swiss Alps during 1961 and 1965. The final results from these measurements (Neckel 2003) are still an important reference and baseline for the SSI from 330 nm to 1099 nm. Reference spectra can be derived from measurements taken during distinct time periods—similar to the data from Labs and Neckel (1967) and the one compiled by Thuillier et al (2004) for two periods in 1992 and 1994, one of which is shown in Figure 2.2. Such spectra are used for many applications, e.g., in weather and climate models. In the VUV range, that is below about 300 nm, such measurements can only be performed from above the atmosphere of the Earth with space probes, satellites, or rockets. Early measurements were obtained by Hinteregger and Hall (1969). For a review see the corresponding articles in White (1977).

Continuous measurements in the ultraviolet (UV) became available with the help of satellite instrumentation in late 1970. Although the radiometric uncertainty was still quite large, the relative variability of the solar VUV irradiance could be determined, mainly because it increases substantially with decreasing wavelength. In the visible regime, however, truly continuous measurements started only with the filter radiometers in 1996 on VIRGO/*SOHO* (Fröhlich et al 1997), and with the spectroradiometers on *SORCE* in 2003 (Rottman et al 2005, 2006)—otherwise one has to rely on measurements at distinct periods of time, such as those

mentioned before. The study of the irradiance variations during the 11-year cycle, on the other hand, requires well sampled time series. An important question for an understanding of the underlying physical mechanisms is how the variation of the TSI is spectrally distributed. This is related to the question of how much of the observed irradiance variations — total and spectral — are changes in luminosity of the Sun or only an angular redistribution of radiance into the direction towards the Earth.

Figure 2.3 demonstrates with the help of a few time series the solar irradiance variability during solar cycles 21 to 23 in wavelength ranges from the visible to X-rays. The data were obtained with space experiments using filter radiometers or spectrometers for the wavelength selection. For comparison, the daily averages of the TSI are plotted in Figure 2.3a as a PMOD composite[6] updated from Fröhlich (2006). Figure 2.3b shows (in light blue) results from the 402 nm VIRGO channel (Fröhlich and Wehrli 2006; Fröhlich 2010) and from SIM (Rottman et al 2005; personal communication J. Harder) with a similar spectral resolution (in dark blue). In Figure 2.3c time series are shown of measurements at 160 nm. The values have been adjusted so that they agree at the solar minima. The red curve is from *SME* (Rottman 1988), the green one from SOLSTICE/*UARS* (Rottman 2000), the light blue one from SUSIM (Floyd et al 1998), and the dark blue one from SOLSTICE/*SORCE* (Rottman et al 2006). Fig. 2.3d: Composite derived for the VUV range near 121 nm as compiled by Woods et al (2000) updated until recently: dark blue is from a model (before 1985 from the radio flux at 10.7 cm, later from the Mg II index), green from *AE-E* (Hinteregger et al 1981), red from *SME*, black from SOLSTICE/*UARS*, light blue from SEE (Woods and Eparvier 2006), and magenta from SOLSTICE. This range contains the very bright H I Lyα line at 121.57 nm and reflects its variations. Fig. 2.3e: Data from SEM (Judge et al 2002) integrated over the 26 nm to 34 nm wavelength range encompassing the bright He II line at 30.4 nm. Fig. 2.3f: The XRS/*GOES* X-ray irradiance from 0.1 nm to 0.8 nm (Kahler and Kreplin 1991; Garcia 1994) (green is the daily median and red the daily maximum). For comparison the XPS/*SORCE* measurements are shown in blue (Woods and Rottman 2005).

The variability of the TSI (Figure 2.3a) can now be compared with the corresponding changes of the SSI in the following panels. The relative variations in the visible and near UV ranges are below 1 % during an 11-year cycle. Since it is very difficult to correct the long-term changes of the instrumentation at these wavelengths reliably, the results must still be regarded as preliminary, although the values of the two time series in panel b agree within a few percent. Note in Figure 2.3c, however, the difference between the behaviour of SUSIM (in light blue) and SOLSTICE (in green) near the year 2000, which indicates a deviation of the long-term calibrations of the instruments.

It is interesting that only the TSI is showing a minimum at the beginning of 2008 with a relative decrease of almost 0.025 % with respect to the other minima. This is about a quarter of the solar cycle amplitude. All the spectral data, however, show almost constant minimum values over the last three solar cycles with relative changes of a few percent of their cycle amplitudes. This may indicate that the solar

[6]For more details see Chapter 32 (Fröhlich 2013).

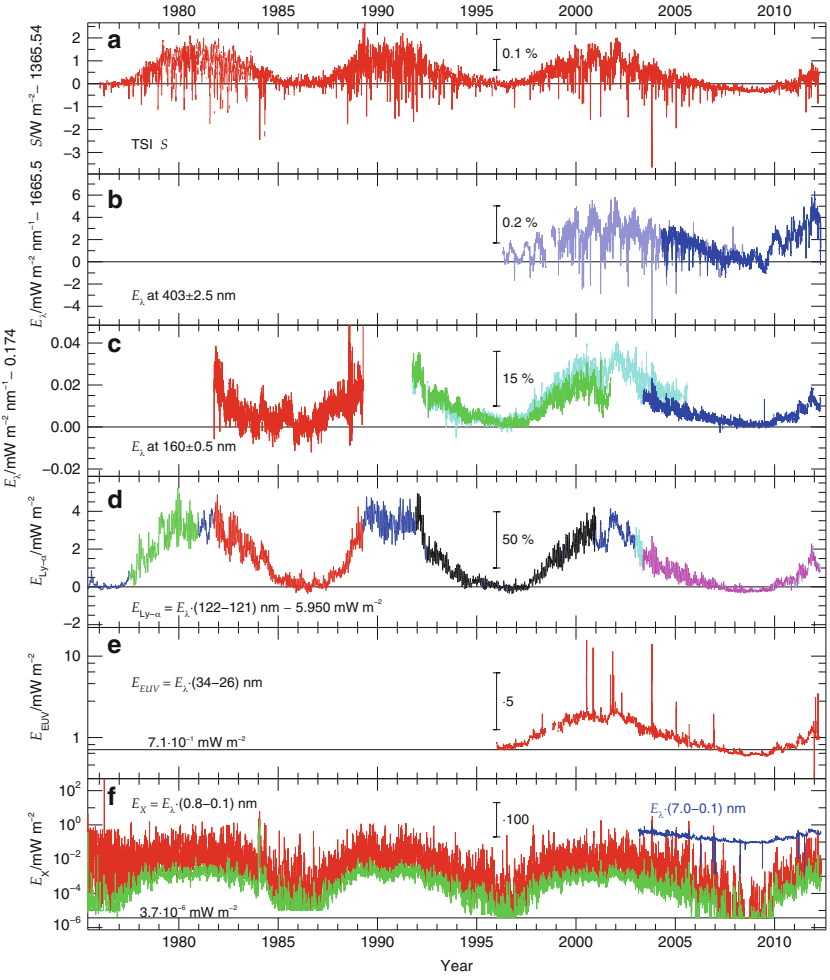

Figure 2.3: **a** TSI composite. The bars in this panel and the following ones indicate relative variations based on the mean values at solar minimum. **b** SSI results from SPM/VIRGO and SIM/*SORCE* in visible light. **c** Time series of SSI in VUV from *SME*, SOLSTICE/*UARS*, SUSIM/*UARS* and SOLSTICE/*SORCE*. **d** Irradiance composite in the range from 121 nm to 122 nm. **e** Extreme-ultraviolet (EUV) irradiance data from SEM/*SOHO* are available for solar cycle 23. The prominent increases correspond to strong flare activity on the Sun. The largest enhancement, for instance, coincides with an X17 flare on 28 October 2003. **f** The XRS/*GOES* X-ray irradiance, and XPS/*SORCE* measurements integrated over a wider range.

cycle variations of TSI and SSI are mainly due to changes in the solar atmosphere related to the prevailing amplitude of the photospheric magnetic fields expanding up to the corona, and that the long-term variations of the TSI are related to contrast changes as function of the magnetic flux density which are only observed in the photosphere and not in the higher atmosphere (see, e.g., Foukal et al 2011; Fröhlich 2012).

Photons in transit

Most of the astronomical objects of interest are far away from the Earth, and the emitted photons have to travel long distances before their detection on a spacecraft. Magnetic or electric fields, unless they are very strong, do not affect photons in vacuum, but gravitational fields influence their propagation. A ray from a star passing close to the Sun will be deflected by $\approx 2''$ (Mikhailov 1959), and gravitational lensing by galaxies or clusters of galaxies is well known for very distant objects. These effects are treated in the general relativity theory (Einstein 1916) that yields a straight propagation path of light only if there are no masses. In this context, it should be mentioned that the travel time of a photon passing near the Sun increases by ≈ 100 µs (Shapiro 1964; Shapiro et al 1971). Both effects are related to a decrease of the speed of light c^* in a region with a gravitational potential

$$\phi = -\frac{G\,M}{R} \tag{2.10}$$

caused by a massive body, where $G = 6.673\,84(80) \times 10^{-11}\ \mathrm{m^3\,kg^{-1}\,s^{-2}}$ is the Newtonian constant of gravitation, M the mass of the body and R the distance from it. The speed c^* then is

$$c^* = c_0 \left(1 + \frac{2\,\phi}{c_0^2}\right) \tag{2.11}$$

(cf., Okun 2000) with a corresponding increase of the momentum p_ν^* in line with Equation 2.5.

Strong gravitational fields can cause significant redshifts. For instance, the relative shift of a spectral line emitted in the photosphere of the Sun observed from the Earth is

$$\frac{\Delta\lambda}{\lambda_0} = \frac{1}{c_0^2}\,\frac{G\,M_\odot}{R_\odot} = -\frac{\phi_\odot}{c_0^2} \approx 2 \times 10^{-6}\ , \tag{2.12}$$

where the mass of the Sun is $M_\odot = 1.989 \times 10^{30}$ kg (cf., e.g., Hentschel 2005). The redshift is, however, *not* a propagation effect, because the photon energy is constant in a static gravitational field (cf., Okun, Selivanov, Telegdi 2000), but depends on the decrease of the energy emitted by atoms at potentials $\phi \neq 0$ (von Laue 1920). The gravitational shift was confirmed in laboratory experiments through the Mössbauer effect (cf., Pound and Rebka 1959) by Cranshaw et al (1960), who stated that from the point of view of a single coordinate system two atomic systems at different gravitational potentials will have different total energies. It was subsequently also observed in the solar spectrum by Blamont and Roddier (1961), Brault (1962,

1963), and Snider (1972, 1974). Hay et al (1960) demonstrated, also with the help of the Mössbauer effect, that an accelerated system caused a redshift as well.

A photon travelling in an inertial system without any interaction with matter will neither change its energy, E_ν, nor its momentum

$$p_\nu = \frac{E_\nu}{c_0} = \frac{h\,\nu}{c_0} \tag{2.13}$$

under the assumption of the validity of energy-mass and momentum conservation laws. Such changes can only occur, when photons are interacting directly or through gravity with matter in the same or other systems.

The Compton effect is an example (see page 34). Another one is the Doppler effect discussed in the next section. There are other effects that affect photons in the presence of matter, e.g., the Faraday rotation of the plane of polarization caused by a magnetic field along the LOS in a plasma (cf., Hutchinson 2002), the Hanle effect discussed in Chapter 33 (Stenflo 2013), and absorption as well as scattering by dust, gas, or plasma regions. A few scattering processes will be described below, but any details are beyond the scope of this chapter.

Doppler effect and aberration

The Doppler effect was originally discovered and formulated for double-star systems (Doppler 1843; Bolzano 1843), and was later verified for sound waves propagating in a medium. In the acoustic case, it was necessary to consider the motions of the transmitter and receiver in the medium separately, because their influences are not symmetric.

For velocities v_t and v_r at angles of ϑ_t and ϑ_r with respect to the direction from the transmitter to the receiver, an emitted frequency, ν, will be received as

$$\nu' = \nu\,\frac{1-(v_\mathrm{r}/c_\mathrm{s})\,\cos\vartheta_\mathrm{r}}{1-(v_\mathrm{t}/c_\mathrm{s})\,\cos\vartheta_\mathrm{t}} \quad , \tag{2.14}$$

where c_s is the speed of sound in the medium.

For electromagnetic waves in vacuum, the special theory of relativity (STR; Einstein 1905b) ascertains that only the relative motion between the transmitter and receiver is of importance. Consider two inertial systems S and S' moving relative to each other with the velocity vector[7], $\boldsymbol{v}_\mathrm{S}$. An emitter of photons with $E = h\,\nu$ is at rest at the origin of system S. An observer at rest in S' sees these photons with $E' = h\,\nu'$ arriving from a certain direction. The Doppler effect and the aberration (also following from the STR) answer the questions related to the frequency and direction changes of electromagnetic radiation with a speed of $c_0 = \nu\,\lambda = \nu'\,\lambda'$ in vacuum. The Doppler formula can be written for a monochromatic electromagnetic wave in its most general form (Einstein 1905b):

$$\nu' = \nu\,\gamma\,(1-\beta\,\cos\vartheta) \quad , \tag{2.15}$$

where ϑ is the angle between the velocity vector and the radiation propagation path. (For $\beta = v_\mathrm{S}/c_0$ and $\gamma = (1-\beta^2)^{-1/2}$, cf., page 22.)

[7] In equations related to Doppler shifts, there is a danger of confusing the frequency symbol, ν, with the relative speed between the inertial systems, v. Therefore, a subscript is used for v in all these cases. Note that $|v_\mathrm{S}| < c_0$, cf., page 22.

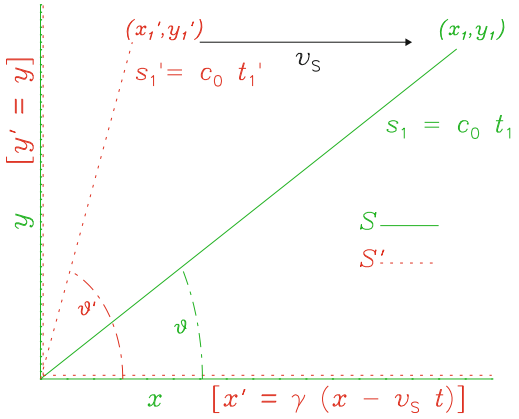

Figure 2.4: The inertial systems S (plotted in green) and S' (red) have parallel coordinate axes. S' is moving with a speed v_S along the positive x-axis of S. Both systems have a common origin at a certain time, $t_0 = 0$, when a photon is emitted there at an angle ϑ in S along a path s_1. The path s_1' in S' will then form an angle ϑ' with the x'-axis. The diagram shows the configuration for the values $\beta = 0.5$ and $\vartheta = 30°$.

The aberration of light was first noticed by Bradley in 1728. The derivation of the relativistic aberration formula

$$\cos\vartheta' = \frac{\cos\vartheta - \beta}{1 - \beta\cos\vartheta} \quad , \tag{2.16}$$

follows from the two Lorentz transformations

$$x' = \gamma\,(x - v_S\,t) \quad \text{and} \quad t' = \gamma\,(t - \beta\,x/c_0) \quad , \tag{2.17}$$

with $\cos\vartheta = x/s_0$ and $\cos\vartheta' = x'/s_0'$ in Figure 2.4.

Doppler and aberration effects are conceptually shown for identical wave packets in Figure 2.5 for various emission angles, ϑ_n, from the origin of S, and $\beta = 0.5$ between S and S_k'. The Doppler shifts resulting from Equation 2.15 are to scale, although it must be kept in mind that they only manifest themselves during the interaction of the photons with matter in the systems S_k'.

There is no aberration for $\vartheta_0 = 0°$ and $\vartheta_4 = 180°$, but, according to Equation 2.15, a longitudinal Doppler effect of

$$\nu' = \nu\,\gamma\,(1 \mp \beta) = \nu\,\sqrt{\frac{1 \mp \beta}{1 \pm \beta}} \tag{2.18}$$

will be observed. On the other hand, there is no Doppler effect for an emission angle θ_0 defined by

$$\cos\theta_0 = (\gamma - 1)/(\gamma\,\beta) \quad . \tag{2.19}$$

However, θ_0 changes to $\theta_0' = 180° - \theta_0$ in the moving system (cf., green line in Figure 2.5). Hovsepyan (1998) demonstrated these relations in a three-dimensional treatment. According to the STR, a corresponding diagram with stationary S_k' (relative to some laboratory system, for instance) and a moving S (with $-v_S$) would give the same results[8].

[8]This situation was considered by Fermi (1932) for the non-relativistic case.

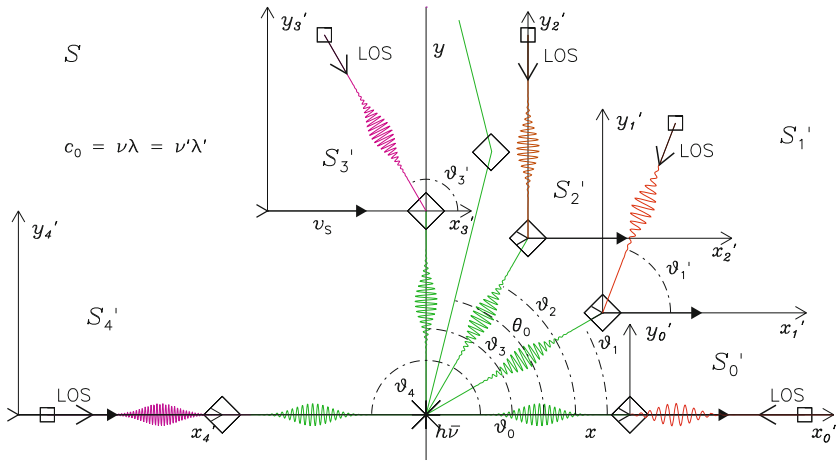

Figure 2.5: Photons are emitted from a source at rest in the inertial system S. The propagation directions from the origin are given by the angles ϑ_0 to ϑ_4. Detectors (indicated by squares) are fixed in the systems S'_k, $k = 0, \ldots, 4$, all moving with a constant velocity, v_S, relative to S parallel to the x axes. The LOS directions of the detectors are indicated by $\vartheta'_k + 180°$ ($\vartheta'_0 = 180°$; $\vartheta'_4 = 0°$). The emitted photons are sketched as green wave packets, and the Doppler-shifted ones in red and violet, respectively. The relative wavelengths and the aberrations are to scale for $\beta = 0.5$. The diamond signs represent some photon-matter interactions in the moving systems. No shift occurs for the angle θ_0 (green line).

Combining Equations 2.15 and 2.16 gives the inverse relativistic Doppler formula

$$\nu = \nu' \gamma \, (1 + \beta \, \cos \vartheta') \quad . \tag{2.20}$$

With $\vartheta' = 90°$, we obtain the transverse Doppler effect

$$\nu' = \nu / \gamma \tag{2.21}$$

in line with the time dilatation, $t = t'/\gamma$; i.e., a clock in S moving with respect to the observer in S' appears to be delayed. Note that from $\cos \vartheta' = 0$ in Equation 2.16 it follows that $\cos \vartheta = \beta$, and Equation 2.15 reduces to Equation 2.21. The name "transverse Doppler effect" is a little misleading, because the relativistic effect does not depend on the angles ϑ and ϑ', and was, in fact, first observed with canal rays moving in both directions along the LOS (Ives and Stilwell 1938, 1941), and later with two-photon spectroscopy in a similar geometry (Kaivola et al 1985).

A detailed discussion of Doppler measurements from binary stars is given by Kopeikin and Ozernoy (1999). Since Einstein derived the relativistic aberration formula in 1905, an endless discussion on its validity with respect to observations of double stars pursued (e.g., Ives 1950; Eisner 1967); recently summarized and emphasized by Puccini and Selleri (2002). To the confusion might have contributed that Einstein (1905b) defined the angle ϑ' (ϕ' in the original) wrongly, although this is obvious from the discussion that follows in Einstein's paper. Many authors have

concluded since that the double-star observations are in conflict with the theory of special relativity. These conclusions are, however, based on a misunderstanding of the physical situation.

Let us consider, without restricting the generality, the simplest configuration: a binary system with equal masses of the components in an orbit coplanar to a circular Earth's orbit. The Sun and the centre of gravity (CG) of the binary system are assumed to be stationary with respect to an inertial system, S'. For observations with largest aberration effects, we then have the requirement that the relevant photons must travel perpendicular to the velocity vectors of the stars and the Earth along the direction from the CG to the Sun, i.e., $\cos\vartheta' = 0$. Yet this does not imply that the light rays are emitted and received at 90° relative to the velocity vectors; a fact that has, of course, been realized by all authors since Bradley for the Earth, but not by all of them for the stars; and there lies the problem.

From Equation 2.16 it follows for the angle of emission

$$\cos\vartheta = \frac{v_\star}{c_0} \quad , \tag{2.22}$$

where $v_\star$ is the orbital velocity of the star considered. For the angle of reception at the Earth, we get

$$\cos\vartheta'' = -\frac{v_\mathrm{E}}{c_0} \quad , \tag{2.23}$$

with v_E the orbital velocity of the Earth. Although the angle ϑ changes with the reversal of $v_\star$, this does not affect ϑ'', in accordance with the observations.

One could argue that the separation into two aberration effects just performed is a trick to save the relativistic aberration formula. It has to be noted, however, that Puccini and Selleri (2002) (and others) also used a trick in their argument by assuming that $v_\star$ and v_E are the consequences of pure translations. If they were, the stars would indeed be seen from the Earth under

$$\cos\vartheta' = -\frac{v_\mathrm{S}}{c_0} = -\frac{v_\mathrm{E} + v_\star}{c_0} \tag{2.24}$$

(cf., S'_3 in Figure 2.5). The second trick is wrong, because the transit times of the photons from the stars to the Earth are much longer than the orbital period of the binary system, whereas the first trick treats the emission locally, and the approximation of $v_\star$ and v_E as translations is nearly perfect.

Photon scattering

In many cases, the propagation directions of photons interacting with matter are changed in some chaotic manner. This process is called scattering, and does not include effects such as reflection, refraction, etc. Usually a distinction is made between coherent and incoherent scattering processes.

Thomson and Rayleigh scattering

In these cases, the scattered photons have the same energy as the original ones, although other parameters (polarization, flux, etc.) might be affected. Since

no energy is transferred, this process is also called elastic scattering. The most important one is scattering on small particles. It is called Thomson scattering for electrons and Rayleigh scattering for other particles small compared to the wavelength. The above formulation assumes that the particles are at rest in the photon-emitting frame. If they are not, the normal Doppler effect (cf., page 30) will occur, but one would still call the process Rayleigh scattering unless there were some additional energy changes. If scattering on larger particles is considered, it is called Mie scattering and exhibits a preferred forward direction.

Compton effect

Photons can interact with electrons through an effect discovered 1922 by Compton (1923). For electrons in matter this interaction is most efficient at energies E_ν between ≈ 10 keV and 1 MeV, for which many electrons in all materials can be considered to be "free" (cf., Chapter 11, Schönfelder and Kanbach 2013). They take up a portion of the energy and momentum of the impinging photon with wavelength λ_0 and cause an incoherent scattering with a wavelength change according to

$$\Delta\lambda = \lambda_1 - \lambda_0 = \frac{h}{m_\mathrm{e}\, c_0}\,(1 - \cos\vartheta) = \frac{2\,h}{m_\mathrm{e}\, c_0}\,\sin^2\frac{\vartheta}{2} \geq 0 \quad , \tag{2.25}$$

where $m_\mathrm{e} = 9.109\,382\,15(45)\times10^{-31}$ kg is the mass of an electron, λ_1 the new wavelength, and ϑ the deflection angle. The wavelength change, $\Delta\lambda$, does not depend on the photon energy and is of the order of the electron Compton wavelength,

$$\lambda_\mathrm{C} = \frac{h}{m_\mathrm{e}\, c_0} = 2.426\,310\,2389(16)\ \mathrm{pm}\ . \tag{2.26}$$

As a note, it should be mentioned that relativistic electrons can scatter on low-energy photons to produce high-energy ones through the inverse Compton effect with $\Delta\lambda < 0$ (cf., Chapters 3 and 4, Kanbach et al 2013; Culhane 2013).

Raman effect

Based on an attempt by Darwin (1923) to explain the optical dispersion phenomenon with quantum physical effects, Smekal (1923) predicted *Translationsquantenübergänge* (translatory quantum transitions) induced by mono-energetic radiation in media with a quasi-periodic atomic structure. The interaction of the radiation with matter would then lead to both energy decreases and increases. These changes were experimentally found by Raman (1928) in many substances. This so-called Raman effect can be observed as radiation scattered with

$$\nu_\mathrm{R} = \nu_\mathrm{o} \pm \nu_\mathrm{s} \quad , \tag{2.27}$$

where ν_o is the irradiating frequency and ν_s is related to the internal oscillations of the medium. Note that, indeed, there are frequency increases as well as decreases.

Fluorescence

In this context, fluorescence might also be mentioned. Here an atom is excited by a high-energy photon and returns to the ground state in several transitions while emitting lower-energy photons. In a unified view, fluorescent and Raman scattering both represent atomic or molecular scattering, for which the initial and final states are different. If such scattering occurs near a resonance, then we speak of fluorescent scattering, while if it is far from a resonance (in the distant line wings), we speak of Raman scattering.

Physical principles of photon detection

The detection process aims at a quantitative determination of the photon flux as a function of the photon energy, its direction, the time of arrival, as well as the polarization characteristics. As for the generation processes, the interactions of photons with matter play a fundamental rôle for their detection.

For the application of the Doppler effect to specific detector designs, we assume that the mass of the receiving device is very much larger than the mass of a photon[9]. Three extreme cases can then be singled out that are of importance in our context:

1. The absorption of a photon by a detector (in general, moving with respect to the radiation source) can be considered as a completely inelastic collision. The total momentum of the detector-photon system will be conserved as well as its energy. Only a certain fraction of the photon energy can be converted into kinetic energy of the detector system in this collision. The remaining portion will be absorbed in other forms of energy. It can be shown that the frequency change of the ensuing Doppler effect just corresponds to the positive or negative kinetic energy transferred to the detector system (cf., e.g., Sommerfeld 1978).

2. The interaction of a photon with a (perfect) mirror as the first element of an optical system represents an elastic collision. This case has been treated by Einstein (1905b) with the result that either the normal Doppler effect is observed, if the photon is subsequently absorbed in the optical system attached to the first element, which will be the usual situation, or, if the photon is observed in the initial system, the Doppler effect can be considered to be applied twice. A mirror receding with v_S in normal incidence will thus cause a frequency change[10] from ν to ν' according to

$$\nu' = \nu \left(\sqrt{\frac{1-\beta}{1+\beta}} \right)^2 = \nu \frac{1-\beta}{1+\beta} \quad . \tag{2.28}$$

3. If the first optical element of a photon analyzer is operating in transmission, the momentum and energy transfer required by the Doppler effect will occur

[9] The details of the transfer of the momentum from the absorbing or emitting systems—usually atomic particles—to the detector device require quantum-mechanical considerations beyond the scope of this chapter (cf., Dicke 1953; Mössbauer 1958).

[10] A typographical error in Einstein's equation has been corrected in Equation 2.28.

at the first encounter with the device. Internally, the Doppler-shifted photon is travelling in the rest frame of the device. Should the final detector, however, be at rest in the initial system, the first Doppler effect would be cancelled by the second one during the absorption.

Irradiance measurements

Conceptually the easiest observation of radiation in space is the determination of the TSI requiring a measurement of the power absorbed by a representation of a black body with known geometry and a relatively crude alignment. The experimental challenge stems from the extreme accuracy required for this measurement, with a relative uncertainty of ideally less than 0.1 %, and even better as far as irradiance variations are concerned (cf., Figure 2.3 and Chapter 32, Fröhlich 2013).

The Sun with a spectral radiance, L_ν, emits perpendicular to a surface element, ΔF, in the frequency and time intervals, $\mathrm{d}\nu$ and Δt, into the solid angle, $\Delta\Omega$, the energy

$$\mathrm{d}Q_\nu = L_\nu \,\mathrm{d}\nu \,\Delta t \,\Delta\Omega \,\Delta F \quad . \tag{2.29}$$

If the radiative properties of the Sun are measured from a moving spacecraft, corrections have to be applied in order to find the quantities for a stationary detector at 1 ua. The normalization with respect to the variable distance is straightforward, because the irradiance varies with the inverse square of the distance, r_E. The velocity correction, however, is more involved:

Since the speeds relative to the Sun are lower than $v_\mathrm{S} \approx 30\ \mathrm{km\,s^{-1}}$, relativistic effects can be neglected. Thus only the radial velocity component, v_r (positive away from the Sun), and linear terms in $\beta_\mathrm{r} = v_\mathrm{r}/c_0$ are of importance. The intervals Δt, $\Delta\Omega$, as well as ΔF are not dependent on v_S in this case.

Equation 2.29 can be written in photon units as

$$\mathrm{d}N_\nu = \mathrm{d}Q_\nu/(h\,\nu) = [L_\nu/(h\,\nu)]\,\mathrm{d}\nu\,\Delta t\,\Delta\Omega\,\Delta F \quad , \tag{2.30}$$

where $\mathrm{d}N_\nu$ is the number of photons in the interval $\mathrm{d}\nu\,\Delta t\,\Delta\Omega\,\Delta F$. The corresponding emission rate is $\mathrm{d}N_\nu/\Delta t$. If it is assumed that the detector collects all photons emitted into $\Delta\Omega$, the detection rate in the moving system will be

$$\frac{\mathrm{d}N'_{\nu'}}{\Delta t} = (1-\beta_\mathrm{r})\,\frac{\mathrm{d}N_\nu}{\Delta t} \quad , \tag{2.31}$$

where the factor $1-\beta_\mathrm{r}$ reflects the geometric correction. Conversion back to energy units yields

$$\mathrm{d}Q'_{\nu'} = (1-\beta_\mathrm{r})\,\frac{\nu'}{\nu}\,\mathrm{d}Q_\nu \tag{2.32}$$

and, with the (classical) Doppler effect (Equation 2.15; $\gamma = 1$),

$$\mathrm{d}Q_\nu = \frac{\mathrm{d}Q'_{\nu'}}{(1-\beta_\mathrm{r})^2} \approx \mathrm{d}Q'_{\nu'}\,(1+2\,\beta_\mathrm{r}) \quad , \tag{2.33}$$

which, after integration over all frequencies, provides the TSI velocity correction used in Chapter 32 (Fröhlich 2013). Similarly, irradiance measurements of stars and other cosmic objects can be performed and corrected.

Spectral solar measurements (radiance and Sun-as-a-star observations; see Figures 2.1 to 2.3) are more complicated, because optical and dispersive systems as well as detectors over a wide spectral range are required with calibrated radiometric responsivity. Moreover, potential variations of the spectral parameters have to be considered, caused, for instance, by relative motions between the emitter and observer, requiring additional corrections. From Equation 2.33, evaluated with the help of Equations 2.15 and 2.29, the correction

$$L_\nu = \frac{L'_{\nu'}}{(1-\beta_\mathrm{r})} \tag{2.34}$$

can be deduced for the spectral radiance and

$$L = \frac{L'}{(1-\beta_\mathrm{r})^2} \tag{2.35}$$

for the radiance. If Equation 2.34 is applied to the Planck law in Equation 2.7, the black-body spectral radiance correction is

$$L_\nu(T) = \frac{L'_{\nu'}(T)}{(1-\beta_\mathrm{r})} \quad . \tag{2.36}$$

A short calculation with the substitution $T = T'/(1-\beta_\mathrm{r})$ and application of the Doppler formula then gives

$$L_\nu(T) = \frac{L'_{\nu'}(T')}{(1-\beta_\mathrm{r})^3} \approx L'_{\nu'}(T')\,(1+3\,\beta_\mathrm{r}) \quad . \tag{2.37}$$

Direction finding

In this section, most of the interactions of photons with matter can completely be described in terms of the classical concepts of electromagnetic radiation as long as no absorption occurs. A specific aspect of this treatment is that the photon propagation can be reversed. The relevant laws of geometric and physical optics can be found in textbooks.

Reflection

The reflection law for polished (metal, glass or similar) surfaces is

$$\alpha_\mathrm{i} = \alpha_\mathrm{r} \quad , \tag{2.38}$$

where the angle of incidence with respect to the normal is α_i and α_r is the angle of reflection. Both rays and the normal lie in one plane. The reflectivity depends on the material and the wavelength. The radiation that is not reflected is absorbed in the material or transmitted.

Dispersion and refraction

Dispersion and refraction laws are of general interest as they govern the propagation of photons in (transparent) matter. For waves, and electromagnetic waves in particular, the phase velocity is defined by

$$c = \frac{\omega}{k} \quad , \tag{2.39}$$

with the angular frequency $\omega = 2\,\pi\,\nu$ and the wave number $k = 2\,\pi/\lambda$. The group velocity is

$$v_{\mathrm{g}} = \frac{\mathrm{d}\omega}{\mathrm{d}k} \quad , \tag{2.40}$$

In transparent media, phase and group velocities are in general functions of the frequency of the waves—a phenomenon called dispersion.

In vacuum, however, there is no dispersion and

$$c = v_{\mathrm{g}} = c_0 \tag{2.41}$$

which follows from

$$c = \frac{\omega_0}{k_0} = \nu_0\,\lambda_0 = c_0 \quad \text{and} \quad v_{\mathrm{g}} = \frac{\mathrm{d}\omega_0}{\mathrm{d}k_0} = c_0 \quad , \tag{2.42}$$

where the index zero indicates a quantity in vacuum, and, in particular, c_0 the speed of light in vacuum as a fundamental constant (cf., pages 22 and 29). With the magnetic constant of the vacuum (also called permeability) $\mu_0 = 4\,\pi \times 10^{-7}\ \mathrm{N\,A^{-2}}$ (exact), the exact electric constant (or permittivity), ε_0, follows from

$$c_0 = \frac{1}{\sqrt{\varepsilon_0\,\mu_0}} \tag{2.43}$$

in Maxwell's equations.

The interaction of photons in a (transparent) medium with the phonons (a description of oscillations in solid materials) leads to a dependence of the propagation velocity on the frequency $\nu = \nu_0$ (which is the same outside and inside the medium). This can be formulated in the wave description as a change in wavelength:

$$\lambda = \frac{\lambda_0}{n} \quad , \tag{2.44}$$

where n, the refractive index, may depend on λ_0 (or ν_0). We then get for the phase velocity

$$c(\nu_0) = \nu_0\,\lambda = \frac{\nu_0\,\lambda_0}{n\,(\nu_0)} = \frac{c_0}{n\,(\nu_0)} \quad , \tag{2.45}$$

and the group velocity is

$$v_{\mathrm{g}} = \frac{\mathrm{d}\omega_0}{\mathrm{d}k} = c_0 \left(n + \nu_0 \frac{\mathrm{d}n}{\mathrm{d}\nu_0} \right)^{-1} = c_0 \left(n - \lambda_0 \frac{\mathrm{d}n}{\mathrm{d}\lambda_0} \right)^{-1} = c \left(1 + \frac{\lambda}{n} \frac{\mathrm{d}n}{\mathrm{d}\lambda} \right) \quad . \tag{2.46}$$

Note the effect of the substitution according to Equation 2.44 on the form of the equation. A dependence of v_g on ω_0 (and λ_0) will lead to a spreading of a pulse of radiation in the medium. If $\mathrm{d}n/\mathrm{d}\lambda_0 < 0$, we have normal dispersion and $v_g < c$. Invoking quantum interference effects, Liu et al (2001) brought a light pulse to a complete stop.

Anomalous dispersion with $\mathrm{d}n/\mathrm{d}\lambda_0 > 0$ and $v_g > c$ can occur under certain resonance conditions of the electromagnetic waves with the atomic elements of the medium. The expression $n_g = n + \nu_0\,\mathrm{d}n/\mathrm{d}\nu_0$ is sometimes called group velocity index (cf., Wang et al 2000). It can become less than one (or even negative), resulting in superluminal light pulse propagation. Under all conditions, however, the signal velocity is defined as the advancement speed of a step function smaller than c_0 (cf., Brillouin 1931), unless evanescent modes are considered (Nimtz and Stahlhofen 2008), which are not relevant in our context. Astronomical observations of propagating fronts with an apparent $v_g > c_0$, so called superluminal motions, can be understood as interactions of wavefronts or jets with spatial structures at angles of nearly 90°with a LOS close to the jet direction (Brillouin 1960; Falla and Floyd 2002).

If a medium with refractive index n is moving at a speed v_S with respect to a laboratory frame, parallel or anti-parallel to the light propagation direction the phase velocity of light inside the medium (as seen from the laboratory) is

$$c' = \frac{c_0}{n} \pm \left(1 - \frac{1}{n^2} - \frac{\lambda_0}{n}\,\frac{\mathrm{d}n}{\mathrm{d}\lambda_0}\right) v_\mathrm{S} \quad , \tag{2.47}$$

known as the Fizeau effect (cf., Einstein 1914).

If electromagnetic radiation travels from one transparent medium to another one, Snell's law

$$n_1 \sin\alpha_1 = n_2 \sin\alpha_2 \tag{2.48}$$

applies, where n_1 and n_2 are the indices of refraction in the media, α_1 is the angle of incidence, and α_2 is the angle of the transmitted ray[11]. In general, both the reflected and the refracted beams are present and partially polarized as given by Fresnel's formulas[12]

$$\phi_\mathrm{r}^\perp = \frac{\sin^2(\alpha_1 - \alpha_2)}{\sin^2(\alpha_1 + \alpha_2)}\,\phi_0^\perp \quad , \tag{2.49}$$

$$\phi_\mathrm{t}^\perp = \frac{\sin 2\alpha_1\,\sin 2\alpha_2}{\sin^2(\alpha_1 + \alpha_2)}\,\phi_0^\perp = \frac{2\,\sin\alpha_1\,\cos\alpha_1\,\sin 2\alpha_2}{\sin^2(\alpha_1 + \alpha_2)}\,\phi_0^\perp \quad , \tag{2.50}$$

$$\phi_\mathrm{r}^\parallel = \frac{\tan^2(\alpha_1 - \alpha_2)}{\tan^2(\alpha_1 + \alpha_2)}\,\phi_0^\parallel \quad , \tag{2.51}$$

and

$$\phi_\mathrm{t}^\parallel = \frac{\sin 2\alpha_1\,\sin 2\alpha_2}{\sin^2(\alpha_1 + \alpha_2)\cos^2(\alpha_1 - \alpha_2)}\,\phi_0^\parallel = \frac{2\,\sin\alpha_1\,\cos\alpha_1\,\sin 2\alpha_2}{\sin^2(\alpha_1 + \alpha_2)\cos^2(\alpha_1 - \alpha_2)}\,\phi_0^\parallel \quad , \tag{2.52}$$

[11] Note that certain materials exhibit a double refraction.

[12] Fresnel's formulas using a complex index of refraction are given in Chapter 9 (Lemaire et al 2013).

where $\phi_0^{\perp}$ is the incident flux polarized perpendicular to the plane of incidence and $\phi_0^{\parallel}$ that polarized in the plane. ϕ_r and ϕ_t are the reflected and transmitted fluxes. For $\alpha_1 = \alpha_2 = 0$ some caution is required in evaluating the limits. Equation 2.49, for instance, can be reformulated with $\sin\alpha_2 = (n_1/n_2)\sin\alpha_1$; $n_2 > n_1$ as:

$$\phi_r^{\perp} = \frac{1 - (n_1/n_2)(\cos\alpha_1/\cos\alpha_2)}{1 + (n_1/n_2)(\cos\alpha_1/\cos\alpha_2)} \quad . \tag{2.53}$$

Equation 2.51 shows that the reflected radiation is completely polarized perpendicular to the plane of incidence if $\alpha_1 + \alpha_2 = 90°$ (Brewster's law). A consequence of Snell's law in Equation 2.48 is the total reflection of radiation in a medium with n_2, if the index n_1 is smaller outside of an interface. Photons impinging under an angle α_2, such that $(n_2 \sin\alpha_2)/n_1 > 1$, cannot leave the denser medium. This effect is the basis of the design of fiber optics.

Attenuation

Radiation is attenuated in any homogeneous medium according to

$$\phi(x) = \phi_0 \exp(-A\,x) \quad , \tag{2.54}$$

where A is the absorption coefficient, ϕ_0 is an initial flux at the position $x_0 = 0$, and x is a linear coordinate along the path of the radiation. Since we are more interested in the transmitted radiation, $\phi(x)$, we can ignore quantum effects in this case, unless single photon experiments are considered. Often the optical depth, τ, is used in this context, giving the path length along which the radiation is attenuated by a factor of e. For homogeneous media, it is $\tau = A^{-1}$.

Sine condition and Fermat's principle

For precise imaging in an optical system with a magnification factor M, Abbe's sine condition $(n_1 \sin\delta_1)/(n_2 \sin\delta_2) = M$ must be fulfilled, where δ_1 and δ_2 are the respective slope angles of a ray from the object point to the image point.

Fermat's principle provides a more general theorem by stating that the optical path length between two points is an extremum. In vacuum light propagates on geodesics; it travels, in fact, on null geodesics as the special relativity theory requires that the eigentime of a photon is zero.

Direction finding concepts

The method of finding the direction of an incoming photon depends very much on the spectral domain. For gamma-rays, no optical systems can be designed, because the reflectivities and refractive indices of all substances are too low. Modulation by masks and other specialized methods, including timing, are required, which will be discussed in Chapter 12 (Hurford 2013). The same is basically true for the hard X-ray range, although so-called Laue lenses (based on Bragg diffraction) and reflective surfaces in grazing incidence have been employed as well. The reflectivity

of smooth surfaces increases in grazing incidence as a consequence of Fresnel's formulas, which show in Equations 2.50 and 2.52 that the transmitted beam becomes evanescent for $\alpha_1 = 90°$ ($\cos\alpha_1 = 0$).

Multilayer coating of the optical surface is another technique for enhancing the reflectivity in a certain wavelength band, and at the same time providing a crude spectral selection (cf., Chapter 9, Lemaire et al 2013). It relies on interferometric amplification of specific bands and attenuation of others. In the soft X-ray regime, multilayer-coated optics can also be used in normal incidence, in addition to optical elements used in grazing incidence. Here and in the VUV range the reflectivities are not very high and, therefore, as few as possible optical surfaces should be used. Silicon carbide (SiC), for instance, probably the best material for use in the VUV, has a significant reflectivity (≥ 0.3) between 60 nm and 300 nm with a maximum of 0.52 at 160 nm.

No material is available for transmission optics in this range, although aluminium has a relatively high transmission from 17 nm to ≈ 84 nm. The transmission limits of some materials at short wavelength are: 155 nm for quartz glass (SiO_2), 122 nm for calcium fluoride (CaF_2); 110 nm for magnesium fluoride (MgF_2); and ≈ 105 nm for lithium fluoride (LiF). Above 120 nm metallic mirrors (Au, Ag, Al) with protective coatings of MgF_2 can be used. Some transmission limits at long wavelength are: 4 µm for SiO_2, 14 µm for NaCl and 23 µm for KCl. Although in the near-UV, visible and near-infrared ranges transmission optics with lenses can be employed, most of the imaging systems are based on reflecting devices, which show less spectral defects and can easier be corrected for astigmatism and other geometric aberrations (cf., Chapter 9, Lemaire et al 2013).

In general, it is much more difficult to build a stigmatic instrument for a wide field of view than for a narrow field close to the optical axis. This axis is, in general, the reference for pointing the optical system in a certain direction. The spacecraft and instrument subsystems must guarantee the pointing accuracy and stability required by the science objectives. A summary of design concepts for VUV instruments and many examples are compiled by Wilhelm et al (2004). Towards longer wavelengths, reflecting telescopes of various design are also the main imaging devices. Of practical importance for the design of a telescope are the various stops: the aperture, defining the opening; the field stop, defining the field of view; and the Lyot stop, internally reducing the diffracted radiation from the aperture.

The angular resolution, δ, achievable in the diffraction-limited case is a function of both the wavelength and the aperture of the instrument, in the sense that it improves with decreasing wavelength and increasing dimensions of the aperture according to $\delta/\mathrm{rad} \approx 0.6\,\lambda/r$, where r is the radius of the aperture. At shorter wavelengths, a higher spatial resolution, i.e., a smaller Airy disk, can thus be obtained with smaller apertures. It is clear that this dependence is related to the wave aspects of the electromagnetic radiation and the corresponding Fraunhofer diffraction effects of apertures on a wave field. Whether the diffraction-limited resolution can be achieved depends critically on the polishing quality of the mirror surface both as far as its figure and micro-roughness are concerned.[13]

[13]Telescopes usually collect radiation in the far-field region of a source, where the diffraction limit is of importance. In the near-field region, however, focusing beyond this limit is possible (cf., e.g., Lerosey et al 2007).

Telescopes are not only required for defining the direction of an incoming photon, and providing imagery in a certain field of view, but also as photon collectors, in particular for faint sources. They operate as radiant flux concentrators. It should, however, be noted that the radiance is constant in an optical system. For high-resolution spatial, temporal, and spectral observations even the solar disk might be considered as a faint source, and the corresponding measurements would be photon-limited unless very large apertures are employed, which are not easy to implement on space missions. Since the radiance of the Sun, in contrast to the irradiance, is not dependent on the observing distance, the situation does not improve by flying closer to the Sun.

Energy discrimination

The next task, after having defined the direction of a photon, is the determination of its energy. Again the energy range, in which the observations are being performed, has a significant influence on the experimental methods to achieve this objective. In the high-energy range, the measurement has to be made in the detector systems themselves (cf., Chapter 21, Smith 2013). In the very low-energy range, i.e., in the microwave energy, discrimination will also be accomplished by the detector systems (cf., Chapter 31, Wild 2013). In the soft X-ray, UV, visible and infrared regimes, dedicated spectral devices can be employed, mostly diffraction gratings, but also prisms and filters, to perform the energy discrimination before the radiation reaches the detector (cf., Chapter 10, Lemaire 2013). The decrease of the index of refraction with increasing wavelength (normal dispersion) is utilized for the spectral analysis in prisms.

The interaction of photons with (non-transparent) material structures is governed by diffraction. In practical applications, Fraunhofer diffraction with parallel rays is distinguished from Fresnel diffraction with inclined rays. Diffraction can completely be understood in the framework of the electromagnetic wave theory. Of fundamental importance in our context is the grating formula (given here for the simple case of a Fraunhofer geometry in reflection)

$$\kappa\,\lambda = d\,(\sin\alpha + \sin\beta) \tag{2.55}$$

where κ is the order of diffraction, d the spacing of the grating, α the angle of incidence and β the angle of reflection (cf., Chapter 10, Lemaire 2013, for a more general approach). Since the spacing, d, can be varied in very wide ranges, spectral discrimination by gratings, in particular by reflection gratings, is useful in many wavelength regimes. Even natural spacings, d, given by the structure of crystals can be invoked in the Bragg diffraction:

$$\kappa\,\lambda = 2\,d\,\sin\theta \quad , \tag{2.56}$$

where θ is the glancing angle.

In order to avoid many reflecting surfaces in VUV application, gratings are often designed in such a way that they can perform, in addition, the functions of optical elements, such as concave mirrors. Filters and prisms obviously are operating in transmission and thus are restricted in their applications.

In most cases, grating and prism devices are designed as slit spectrographs. They provide a good spectral resolution in a wide range, but use the photons collected by the telescope rather inefficiently. In particular, the imaging of extended areas in spatially-resolved observations requires a scanning motion of the slit perpendicular to its length, which is very time consuming. Slitless spectrographs are more effective in this context, but can only be used for strong spectral lines in an otherwise relatively flat spectral regime, because spatial and spectral regimes are superimposed. Two-dimensional spectroscopy employing interferometers is the choice for fast instruments operating in a restricted wavelength range (cf., Chapters 16 to 19, Lindegren 2013; Quirrenbach 2013; Griffin and Ade 2013; Title 2013). As long as transmission optics are available, such systems are relatively easy to implement, but in the VUV range the design and development of interferometers are challenging tasks.

For all systems depending on interference methods, the coherency of the radiation under study is of critical importance. The standard coherence condition for Young's double slit configuration is $2\,d\,\sin\epsilon \ll \lambda$, where d is the separation of the slits, ϵ is the half-opening angle of the beam and λ is the wavelength of the radiation (Verdet's coherence condition). The same condition is applicable to slit spectrometer using gratings, where d is then equal to the slit width. If, however, the spectrometer provides a stigmatic image of the slit on the detector, the optical performance of the spectrometer has to be considered in detail. It is of interest here that the time of arrival of photons is correlated in coherent radiation (Hanbury Brown and Twiss 1956a). This can be used in an intensity interferometer to measure radii of stars (Hanbury Brown and Twiss 1956b). These observations had a great influence on the development of the quantum theory of optical coherence (Glauber 1963). It is also noteworthy that interference of radiation from two lasers has been observed (Louradour et al 1993).

Photon detectors

Modern detectors mounted on spacecraft systems have to transform, in some way, a photon impact into digital information that can be recorded and telemetered to the ground. Most of them are two-dimensional devices composed of many pixels, i.e., picture elements, of a certain size. Pixels can be geometrically defined, but virtual pixels generated by the readout algorithm are also possible. This pixel size has to be adjusted to the capabilities of the telescope and spectrometer, and then determines the resolution in both dimensions corresponding in general, to the spatial and spectral domains. Resolving powers are usually defined for both regimes by $p_x = x/\delta x$ and $p_\lambda = \lambda/\delta\lambda$, respectively. Equating δx and $\delta\lambda$ with the pixel size and considering the sampling theorem would indicate a spatial resolution of $\approx 2\,\delta x$ and a spectral of $\approx 2\,\delta\lambda$. It is of great importance for the analysis of spectra that the shift and broadening of spectral lines can be determined with sub-pixel resolution, provided the line width is wider than several pixels. The details depend on the signal-to-noise ratio, but typically the shift can be measured to one tenth of a pixel (cf., Wilhelm et al 1995). An important distinction between types of detectors is whether they are photon-counting devices or integrating systems.

Quantum efficiency

A critical performance measure of any photon detector is its quantum efficiency (QE) as a function of wavelength, $\eta(\lambda)$. The definition of this quantity in the literature varies; here we use the ratio:

$$\eta = \frac{C}{N} \tag{2.57}$$

where C is the number of counted events and N the number of incoming photons. The efficiency is in general a strong function of the photon energy, but may depend on other parameters as well. In general, the QE has to be determined by applying a radiometrically-calibrated photon flux and comparing it with the output counts (cf., Chapter 36, Huber et al 2013). However, Rarity et al (1987) performed QE measurements without a calibration standard. They used the parametric down conversion of a photon with wavelength λ_0 into two photons with λ_1 and λ_2 in a non-linear crystal. Two detectors properly placed would count the down-converted photons as $N_1 = \eta(\lambda_1)\, P$ and $N_2 = \eta(\lambda_2)\, P$, where P is number of photon pairs created. The coincidence counts would be

$$C = \eta(\lambda_1)\, \eta(\lambda_2)\, P \tag{2.58}$$

and thus $\eta(\lambda_1) = C/N_2$ and $\eta(\lambda_2) = C/N_1$.

Photon absorption

A brief survey of the primary interaction processes is given here, all of which are based on the absorption (or rather the demolition) of the photon to be detected.[14] The absorption is a strong function of the photon energy and, of course, heavily depends on the detector material under consideration. It is clearly related to the attenuation of radiation treated on page 40, but here we are more interested in the effects of the individual photon absorption event. Once a photon interacts with the detector system, various amplification and measuring schemes have to be employed as detailed in the other chapters of this book.

Photo effect The photo effect, or more exactly, the external photo-electric effect, is one of the most important interaction processes of photons with opaque matter in photon detectors. The effect was discovered by Hertz (1887) and Hallwachs (1888), studied in detail by Lenard (1902), explained by Einstein (1905a) and experimentally confirmed by Millikan (1916). A photon with energy $h\,\nu$, impinging on the surface of a material, can release an electron with a maximal energy of

$$W_{\max} = h\,\nu - W_{\mathrm{A}} \quad , \tag{2.59}$$

where W_{A} is an electron work function characteristic of a given material[15]. Typical values are between $W_{\mathrm{A}} \approx 2$ eV and 6 eV.

[14] For completeness it should be mentioned that non-demolition measurements of single photons were accomplished (Nogues et al 1999), as well as electric field measurements at sub-photon levels (Brune et al 1994; Foster et al 2002).

[15] Note that time-delayed photo effects have been observed for semi-transparent photocathodes that are not in line with Equation 2.59 (Billard and Burns 1983).

Pair Production At energies above $E_\nu = 1.02$ MeV, i.e., twice the equivalent mass of an electron, m_e, a photon can produce an electron-positron pair in the electric field of a nucleus. The nucleus is required for momentum conservation. The pair production efficiency increases with the photon energy and the interaction cross-section is proportional to Z^2, with the Z charge number of the nucleus. The electron-positron pairs then have to be recorded by appropriate means (cf., Chapter 11, Schönfelder and Kanbach 2013). Pair production also occurs in the Coulomb field of electrons albeit with much smaller cross-sections.

Solid-state detectors and scintillation counters In solid-state detectors, with donor and acceptor regions forming n-p junctions, the internal photo effect creates electrons and electron holes that can be collected and counted (cf., e.g., Chapters 25 and 26, Schühle 2013; Schühle and Hochedez 2013).

In the X-ray and gamma-ray regimes, scintillation detectors are in frequent use (cf., Chapter 21, Smith 2013). The high-energy photons, through the internal photo effect, ionize atoms in certain crystallic materials. The recombination events of the atoms and electrons then produce a large number of optical photons that can be collected by standard photomultipliers. Na J and Cs J crystals have frequently been employed in the past. Modern detectors work with $Gd_2\,Si\,O_5$ (GSO) and $Bi_4\,Ge_3\,O_{12}$ (BGO) crystals, which are not hygroscopic and have different rise and decay times facilitating pulse discrimination (cf., e.g., Takahashi et al 2007).

Photon detectors based on superconductivity Many modern photon detectors employ superconductive material. Although this chapter cannot discuss the physics of superconductivity in any detail, a few important concepts will be mentioned as well as their application in photon detectors.

Cooper pairs Cooper (1956) suggested that electrons (as fermions) in superconducting metallic materials form pairs—later to be called Cooper pairs—due to an electron-phonon interaction at low temperatures, which could overcome the Coulomb repulsion of the electrons. The resulting bosons would be responsible for the superconductive properties, but might easily split into two electrons by an external excitation. Even photons with an energy of a few millielectronvolts can break up a Cooper pair into the electrons, which then have to be collected by suitable circuitry. This could, for instance, be a superconducting tunnel junction (STJ); see Perryman et al (1993), Peacock et al (1996), and also Chapter 27 (Martin and Verhoeve 2013).

Microcalorimeters Superconducting devices can also be employed to measure the heat input of single photons from the infrared to gamma-ray ranges. Typical detectors are designed as transition edge sensors (TES) (cf., Chapters 28 and 29, Porter 2013; Eaton 2013). The absorbed photon energy is thermalized and leads to a large increase in resistance of the detector material that is biased close to the superconducting-normal transition edge. Details on the energy resolution and dead times achieved can be found in Irwin et al (1998) and Romestain et al (2004).

Heterodyne receivers In the sub-millimetre regime and at longer wavelengths, the photon concept is only of theoretical interest. The receivers and detectors are designed for the analysis of long-wavelength electromagnetic radiation employing heterodyne techniques (cf., Chapter 31, Wild 2013). A low noise temperature is of paramount importance in such systems. Superconductor-insulator-superconductor (SIS) tunnel junctions with their low band gaps are useful in this context.

Closing summary

The interaction of photons with matter during both the emission and the absorption processes is considered in this chapter as an introduction to the following chapters. The physics involved in the transfer phase of the photons from the astronomical source region to their detection near the Earth is outlined as well. The radiation from the Sun is discussed in some detail as an example. The physics of entangled photons, on the other hand, is only briefly mentioned, as applications to astrophysical observations are rather limited at this stage.

References

Adenier G (2008) Quantum entanglement, fair sampling, and reality: Is the moon there when nobody looks? Am J Phys 76:147–152

Aharonov Y, Bohm D (1961) Time in the quantum theory and the uncertainty relation for time and energy. Phys Rev 122:1649–1658

Amsler C, Doser M, Antonelli M (plus 170 authors)(2008) Review of particle physics. Phys Lett B 667:1–1340

Avrett EH, Kurucz RL, Loeser R (2006) Identification of the broad solar emission features near 117 nm. Astron Astrophys 452:651–655

Ayres TR (2000) The *SOHO*-stellar connection. Sol Phys 193:273–297

Bell JS (1964) On the Einstein–Podolsky–Rosen paradox. Physics 1:195–200

Billard TC, Burns G (1983) Time-delayed photoelectric effect. Nature 306:247–248

Blamont JE, Roddier F (1961) Precise observation of the profile of the Fraunhofer strontium resonance line. Evidence for the gravitational redshift on the Sun. Phys Rev Lett 7:437–440

Bolzano B (1843) Ein paar Bemerkungen über eine neue Theorie in Herrn Professor Chr. Doppler's Schrift. Ann Phys (Leipzig) 136:83–88

Born M, Wolf E (1999) Principles of optics. Electromagnetic theory of propagation, interference and diffraction of light (7th edition). Cambridge University Press, Cambridge New York

Born M, Heisenberg W, Jordan P (1926) Zur Quantenmechanik. II. Z Phys 35: 557–615

Bose SN (1924) Plancks Gesetz und Lichtquantenhypothese. Z Phys 26:178–181

Brault JW (1962) The gravitational redshift in the solar spectrum. PhD Diss, Princeton University

Brault J (1963) Gravitational redshift of solar lines. Bull Am Phys Soc 8:28

Brillouin L (1931) Die Quantenstatistik. Verlag von Julius Springer, Berlin

Brillouin L (1960) Wave propagation group velocity. Academic Press Inc, New York, London
Brugel EW, Shull JM, Seab CG (1982) The ultraviolet spectrum of Herbig-Haro object 2H. Astrophys J 262:L35–L39
Brune M, Nussenzveig P, Schmidt-Kahler F (plus four authors) (1994) From Lamb shift to light shift: Vacuum and subphoton cavity fields measured by atomic phase sensitive detection. Phys Rev Lett 72:3339–3342
Bureau International des Poids et Mesures (BIPM) (2006) Le Système International d'Unités (SI). 8^{e} édition, Sèvres
Carretti E, Rosset C (2013) Polarization measurements of the Cosmic Microwave Background. ISSI SR-009:617–627
Casimir HBG (1949) Sur les forces van der Waals–London. J Chim Phys 46:407–410
Clauser JF, Horn MA, Shimony A, Holt RA (1969) Proposed experiment to test local hidden-variable theories. Phys Rev Lett 23:880–884
Compton AH (1923) A quantum theory of the scattering of X-rays by light elements. Phys Rev 21:483–502
Cooper LN (1956) Bound electron pairs in degenerate Fermi gas. Phys Rev 104:1189–1190
Cranshaw TE, Schiffer JP, Whitehead AB (1960) Measurement of the gravitational red shift using the Mössbauer effect in Fe^{57}. Phys Rev Lett 4:163–164
Culhane JL (2013) X-ray astronomy: energies from 0.1 keV to 100 keV. ISSI SR-009:73–91
Darwin CG (1923) The wave theory and the quantum theory. Nature 111:771–773
Dicke RH (1953) The effect of collisions upon the Doppler width of spectral lines. Phys Rev 89:472–473
Dicke RH, Peebles PJE, Roll PG, Wilkinson DT (1965) Cosmic black-body radiation. Astrophys J 142:414–419
Dirac PAM (1927) The quantum theory of the emission and absorption of radiation. Proc Roy Soc London A 114:243–265
Doppler CA (1843) Über das farbige Licht der Doppelsterne und einiger anderer Gestirne des Himmels. Abh königl böhm Ges Wiss 2:465–482
Eaton HAC (2013) Infrared imaging bolometers. ISSI SR-009:515–524
Ehrenfest P (1925) Energieschwankungen im Strahlungsfeld oder Kristallgitter bei Superposition quantisierter Eigenschwingungen. Z Phys 34:362–373
Einstein A (1905a) Über einen die Erzeugung und Verwandlung des Lichtes betreffenden heuristischen Gesichtspunkt. Ann Phys (Leipzig) 322:132–148
Einstein A (1905b) Zur Elektrodynamik bewegter Körper. Ann Phys (Leipzig) 322:891–921
Einstein A (1905c) Ist die Trägheit eines Körpers von seinem Energieinhalt abhängig? Ann Phys (Leipzig) 323:639–641
Einstein A (1914) Bemerkungen zu Paul Harzers Abhandlung "Über die Mitführung des Lichtes im Glas und die Aberration". Astron Nachr 1999:7–10
Einstein A (1916) Die Grundlage der allgemeinen Relativitätstheorie. Ann Phys (Leipzig) 354:769–822
Einstein A (1917) Zur Quantentheorie der Strahlung. Phys Z 18:121–128

Einstein A, Stern O (1913) Einige Argumente für die Annahme einer molekularen Agitation beim absoluten Nullpunkt. Ann Phys (Leipzig) 345:551–560
Einstein A, Podolsky B, Rosen N (1935) Can quantum-mechanical description of physical reality be considered complete? Phys Rev 47:777–780
Eisner E (1967) Aberration of light from binary stars—a paradox? Am J Phys 35:817–819
Falla DF, Floyd MJ (2002) Superluminal motion in astronomy. Eur J Phys 23:69–81
Fermi E (1932) Quantum theory of radiation. Rev Mod Phys 4:87–132
Floyd L, Reiser P, Crane P (plus three authors) (1998) UV measurements from SUSIM on *UARS*. Sol Phys 177:79–86
Foukal P, Ortiz A, Schnerr R (2011) Dimming of the 17th Century Sun. Astrophys J 733:L38, DOI: 10.1088/2041-8205/733/2/L38
Foster GT, Smith WP, Reiner JE, Orozco LA (2002) Time-dependent electric field fluctuations at the subphoton level. Phys Rev A 66:033807-1–12
Fröhlich C (2006) Solar irradiance variability since 1978: Revision of the PMOD composite during solar cycle 21. Space Sci Rev 125:53–65
Fröhlich C (2010) Spectral solar irradiance over solar cycle 23 from sunphotometers of VIRGO on *SOHO*. AGU Fall Meeting, available at ftp://ftp.pmodwrc.ch/pub/Claus/AGU_Fall2010/GC33C-08.ppt
Fröhlich C (2012) Total solar irradiance observations. Surveys Geophys 33 (3–4):453–473
Fröhlich C (2013) Solar radiometry. ISSI SR-009:565–581
Fröhlich C, Wehrli C (2006) Comparison of the WRC85 solar spectral irradiance with RSSV1 and the SPM of VIRGO/*SOHO*. In: *SORCE* Science Meeting, 19-22 September 2006, San Juan Islands, Washington, USA. Poster available from ftp://ftp.pmodwrc.ch/pub/Claus/SORCE-2006/SSI_poster.pdf
Fröhlich C, Crommelynck D, Wehrli C (plus seven authors) (1997) In-flight performances of VIRGO solar irradiance instruments on *SOHO*. Sol Phys 175:267–286
Fröhlich C, Huber MCE, Solanki S, von Steiger R (eds) (1998) Solar composition and its evolution – From core to corona, Space Sci Ser ISSI, Vol 5. Kluwer Academic Publishers, Dordrecht, and Space Sci Rev 85, Nos. 1-2, 1998
Garcia HA (1994) Temperature and emission measure from *GOES* soft X-ray measurements. Sol Phys 154:275–308
Glauber RJ (1963) The quantum theory of optical coherence. Phys Rev 130:2529–2539
Glauber RJ (2007) Quantum theory of optical coherence (selected papers and lectures). Wiley-VCH Verlag, Weinheim
Goldhaber AS, Nieto MM (1971) Terrestrial and extraterrestrial limits on the photon mass. Rev Mod Phys 43:277–296
Griffin MJ, Ade PAR (2013) Narrow-band imaging by use of interferometers. ISSI SR-009:333–347
Hajdas W, Suarez-Garcia E (2013) Polarimetry at high energies. ISSI SR-009:599–615
Hallwachs W (1888) Über den Einfluss des Lichtes auf elektrostatisch geladene Körper. Ann Phys Chem 269:301–312
Hanbury Brown R, Twiss RQ (1956a) Correlation between photons in two coherent beams of light. Nature 177:27–29

Hanbury Brown R, Twiss RQ (1956b) A test of a new type of stellar interferometer on Sirius. Nature 178:1046–1048

Hay HJ, Schiffer JP, Cranshaw TE, Egelstaff PA (1960) Measurement of the red shift in an accelerated system using the Mössbauer effect in Fe^{57}. Phys Rev Lett 4:165–166

Heisenberg W (1927) Über den anschaulichen Inhalt der quantentheoretischen Kinematik und Mechanik. Z Phys 43:172–178

Hentschel K (2005) Testing relativity. In: Physics before and after Einstein (M. Mamone Capria ed.). IOS Press, Amsterdam pp. 163–182

Hertz H (1887) Über einen Einfluss des ultravioletten Lichtes auf die elektrische Entladung. Wied Ann 31:983–1000

Hilgevoord J (1996) The uncertainty principle for energy and time. Am J Phys 64:1451–1456

Hilgevoord J (1998) The uncertainty principle for energy and time. II. Am J Phys 66:396–402

Hinteregger HE, Hall LA (1969) Solar extreme ultraviolet emissions in the range 260 to 1300 Å observed from *OSO-III*. Sol Phys 6:175–182,

Hinteregger HE, Fukui K, Gilson BR (1981) Observational, reference and model data on solar EUV, from measurements on *AE-E*. Geophys Res Lett 8:1147–1150

Hong CK, Ou ZY, Mandel L (1987) Measurement of subpicosecond time intervals between two photons by interference. Phys Rev Lett 59: 2044–2046

Hovsepyan YI (1998) Some notes on the relativistic Doppler effect. Phys Uspekhi 41:941–944

Huber MCE, Pauluhn A, Timothy JGT, Zehnder A (2013) Calibration. ISSI SR-009:629–638

Hurford GJ (2013) X-Ray imaging with collimators, masks and grids. ISSI SR-009:243–254

Hutchinson IH (2002) Principles of plasma diagnostics (2nd edition). Cambridge University Press, Cambridge New York Melbourne Madrid Cape Town

Irwin KD, Hilton GC, Wollman DA, Martinis JM (1998) Thermal-response time of superconducting transition-edge microcalorimeters. J Appl Phys 83:3978–3985

Ives HE (1950) Extrapolation from the Michelson-Morley experiment. J Opt Soc Am 40:185–191

Ives HE, Stilwell GR (1938) An experimental study of the rate of a moving atomic clock. J Opt Soc Am 28:215–226

Ives HE, Stilwell GR (1941) An experimental study of the rate of a moving atomic clock. II. J Opt Soc Am 31:369–374

Jackson JD (1999) Classical electrodynamic (3rd edition). John Wiley & Sons, New York etc.

Judge DL, Ogawa HS, McMullin DR (plus two authors) (2002) The *SOHO* CELIAS/SEM EUV database from SC23 minimum to the present. Adv Space Res 29:1963–1968

Kahler SW, Kreplin RW (1991) The NRL *SOLRAD* X-ray detectors – A summary of the observations and a comparison with the SMS/*GOES* detectors. Sol Phys 133:371–384

Kaivola M, Poulsen O, Riis E, Lee SA (1985) Measurements of the relativistic Doppler shift in neon. Phys Rev Lett 54:255–258

Kanbach G, Schönfelder V, Zehnder A (2013) High-energy astrophysics—energies above 100 keV. ISSI SR-009:55–72

Kopeikin SM, Ozernoy LM (1999) Post-Newtonian theory for precision Doppler measurements of binary star orbits. Astrophys J 523:771–785

Labs D, Neckel H (1962) Die absolute Strahlungsintensität der Sonnenmitte im Spektralbereich $4010 \leq \lambda \leq 6569$ Å. Z Astrophys 55:269–289

Labs D, Neckel H (1967) Die absolute Strahlungsintensität der Mitte der Sonnenscheibe im Spektralbereich $3288 \leq \lambda \leq 12\,480$ Å. Z Astrophys 65:133–185

Lamarre JM, Dole H (2013) The Cosmic Microwave Background. ISSI SR-009:165–183

Lamb WE, Jr (1995) Anti-photon. Appl Phys B 60:77–84

von Laue M (1920) Zur Theorie der Rotverschiebung der Spektrallinien an der Sonne. Z Phys 3:389–395

Lemaire P (2013) Normal- and grazing-incidence gratings and mountings used in space. ISSI SR-009:211–223

Lemaire P, Aschenbach BA, Seely JF (2013) Space telescopes. ISSI SR-009:183–210

Lenard P (1902) Über die lichtelektrische Wirkung. Ann Phys (Leipzig) 313: 149–199

Lerosey G, de Rosny J, Tourin A, Fink M (2007) Focusing beyond the diffraction limit with far-field time reversal. Science 315:1120–1122

Lindegren L (2013) High-accuracy positioning: astrometry. ISSI SR-009:299–311

Liu C, Dutton Z, Behroozi CH, Hau LV (2001) Observation of coherent optical information storage in an atomic medium using halted light pulses. Nature 409: 490–493

Louradour F, Reynaud F, Colombeau B, Froehly C (1993) Interference fringes between two separate lasers. Am J Phys 61:242–245

Mandelstam LI, Tamm IE (1945) The uncertainty relation between energy and time in non-relativistic quantum mechanics. J Phys (USSR) 9:249–254

Martin DDE, Verhoeve P (2013) Superconducting tunnel junctions. ISSI SR-009:479–496

Mather JC, Cheng ES, Eplee RE, Jr. (plus 18 authors) (1990) A preliminary measurement of the Cosmic Microwave Background spectrum by the *Cosmic Background Explorer (COBE)* satellite. Astrophys J 354:L37–L40

Mather JC, Cheng ES, Cottingham DA (plus 20 authors) (1994) Measurement of the Cosmic Microwave Background spectrum by the *COBE* FIRAS instrument. Astrophys J 420:439–444

Mikhailov AA (1959) The deflection of light by the gravitational field of the Sun. Mon Not R Astr Soc 119:593–608

Millikan RA (1916) A direct photoelectric determination of Plank's "h". Phys Rev 7:355–390

Mohideen U, Roy A (1998) Precision Measurement of the Casimir force from 0.1 to 0.9 µm. Phys Rev Lett 81:4549–4552

Mohr PJ, Taylor BN, Newell DB (2008) CODATA recommended values of the fundamental physical constants: 2006. arXiv:0801.0028

Mössbauer RL (1958) Kernresonanzfluoreszenz von Gammastrahlung in Ir^{191}. Z Physik 151:124–143

Neckel H (2003) On the Sun's absolute disk-center and mean disk intensities, its limb darkening, and its 'limb temperature' ($\lambda\lambda$330 to 1099 nm). Sol Phys 212:239–250

Nimtz G, Stahlhofen AA (2008) Universal tunneling time for all fields. Ann Phys (Berlin) 17:374–379

Nisius R (2000) Photon structure from deep inelastic electron-photon scattering. Phys Rep 332:165–317

Nogues G, Rauschenbeutel A, Osnaghi S (plus three authors) (1999) Seeing a single photon without destroying it. Nature 400:239–242

Okun LB (1989) The concept of mass. Phys Today 42(60):31–36

Okun LB (2000) Photons and static gravity. Mod Phys Lett A 15(31):1941–1947

Okun LB, Selivanov KG, Telegdi VL (2000) On the interpretation of the redshift in a static gravitational field. Am J of Phys 68(2):115–119

Peacock A, Verhoeve P, Rando N (plus nine authors) (1996) Single optical photon detection with a superconducting tunnel junction. Nature 381:135–137

Penzias AA, Wilson RW (1965) A measurement of excess antenna temperature at 4080 Mc/s. Astrophys J 142:419–421

Perryman MAC, Foden CL, Peacock A (1993) Optical photon counting using superconducting tunnel junctions. Nucl Instrum Methods Phys Res Sect A 325: 319–325

Planck M (1900) Über irreversible Strahlungsvorgänge. Ann Phys (Leipzig) 306: 69–122

Planck M (1901) Über das Gesetz der Energieverteilung im Normalspektrum. Ann Phys (Leipzig) 309:553–563

Planck M (1909) Zur Theorie der Wärmestrahlung. Ann Phys (Leipzig) 336: 758–768

Porter FS (2013) X-ray calorimeters. ISSI SR-009:497–514

Pound RV, Rebka GA (1959) Gravitational red-shift in nuclear resonance. Phys Rev Lett 3:439–441

Puccini GD, Selleri F (2002) Doppler effect and aberration of light from the point of view of absolute motion. Nuovo Cim 117 B:283–293

Quirrenbach A (2013) Interferometric imaging from space. ISSI SR-009:313–332

Raman CV (1928) A new radiation. Ind J Phys 2:387–398

Rarity JG, Ridley KD, Tapster PR (1987) Absolute measurement of detector quantum efficiency using parametric down-conversion. Appl Opt 26:4616–4619

Romestain R, Delaet B, Renaud-Goud P (plus four authors) (2004) Fabrication of a superconducting niobium nitride hot electron bolometer for single-photon counting. New J Phys 6:129-1–15

Rottman GJ (1988) Observations of solar UV and EUV variability. Adv Space Res 8:53–66

Rottman G (2000) Variations of solar ultraviolet irradiance observed by the *UARS* SOLSTICE – 1991 to 1999. Space Sci Rev 94:83–91

Rottman G, Harder J, Fontenla J (plus three authors) (2005) The spectral irradiance monitor (SIM): Early observations. Sol Phys 230:205–224

Rottman GJ, Woods TN, McClintock W (2006) *SORCE* solar UV irradiance results. Adv Space Res 37:201–208

Schönfelder V, Kanbach G (2013) Imaging through Compton scattering and pair creation. ISSI SR-009:225–242
Schühle U (2013) Intensified solid state sensor cameras: ICCD and IAPS. ISSI SR-009:455–465
Schühle U, Hochedez J-F (2013) Solar-blind UV detectors based on wide band gap semiconductors. ISSI SR-009:467–477
Shapiro II (1964) Fourth test of general relativity. Phys Rev Lett 26:789–791
Shapiro II, Ash ME, Ingalls RP, Smith WB, Campbell DB, Dyce RB, Jurgens RF, Pettengill GH (1971) Fourth test of general relativity: New radar result. Phys Rev Lett 26:1132–1135
Smekal A (1923) Zur Quantentheorie der Dispersion. Naturwissenschaften 43: 873–875
Smith DM (2013) Hard X-ray and gamma-ray detectors. ISSI SR-009:367–389
Snider JL (1972) New measurement of the solar gravitational red shift. Phys Rev Lett 28:853–856
Snider JL (1974) Comments on two recent measurements of the solar gravitational red-shift. Sol Phys 36:233–234
Sommerfeld A (1978) Optik, Verlag Harri Deutsch, Thun, Frankfurt/Main.
Stenflo JO (2013) Stokes polarimetry of the Zeeman and Hanle effects. ISSI SR-009:583–598
Strekalov DV, Pittman TB, Shih YH (1998) What we can learn about single photons in a two-photon interference experiment. Phys Rev A 57:567–570
Sunyaev RA, Zel'dovich YB (1980) Microwave background radiation as a probe of the contemporary structure and history of the universe. Ann Rev Astron Astrophys 18:537–560
Takahashi T, Abe K, Endo M (plus 67 authors) (2007) Hard X-ray detector (HXD) on board *Suzaku*. Publ Astron Soc Japan 59:35–51
Thuillier G, Floyd L, Woods T (plus four authors) (2004) Solar irradiance reference spectrum. In: Geophysical Monograph 141: Solar variability and its effect on climate, American Geophysical Union, Washington DC, USA, pp. 171–194
Title AM (2013) Michelson interferometers. ISSI SR-009:349–361
Tiwari SC (2002) Relativity, entanglement and the physical reality of the photon. J Opt B Quantum Semiclass Opt 4:S39–S46
Wang LJ, Kuzmich A, Dogariu A (2000) Gain-assisted superluminal light propagation. Nature 406:277–279
White OR (1977) The solar output and its variations. Colorado Associated University Press, Boulder, USA
Wild W (2013) Coherent far-infrared / submillimeter detectors. ISSI SR-009:543–564
Wilhelm K, Curdt W, Marsch E (plus 13 authors) (1995) Some design and performance features of SUMER. Proc SPIE 2517:2–11
Wilhelm K, Schühle U, Curdt W (plus four authors) (2002) Solar vacuum-ultraviolet radiometry with SUMER. ISSI SR-002:145–160
Wilhelm K, Dwivedi BN, Marsch E, Feldman U (2004) Observations of the Sun at vacuum-ultraviolet wavelengths from space. Part I. Space Sci Rev 111:415–480
Woods TN, Rottman G (2005) XUV photometer system (XPS): Solar variations during the *SORCE* mission. Sol Phys 230:375–387

Woods TN, Eparvier FG (2006) Solar ultraviolet variability during the *TIMED* mission. Adv Space Res 37:219–224

Woods TN, Tobiska WK, Rottman GJ, Worden JR (2000) Improved solar Lyman-α irradiance modeling from 1947 through 1999 based on *UARS* observations. J Geophys Res 105:27 195–27 216

Zbinden H, Brendel J, Tittel W, Gisin N (2001) Experimental test of relativistic quantum state collapse with moving reference frames. J Phys A Math Gen 34:7103–7109

http://www.springer.com/978-1-4614-7803-4

Observing Photons in Space
A Guide to Experimental Space Astronomy
Huber, M.C.E.; Pauluhn, A.; Culhane, J.L.; Timothy, J.G.;
Wilhelm, K.; Zehnder, A. (Eds.)
2013, XVI, 731 p. 313 illus., 161 illus. in color.,
Hardcover
ISBN: 978-1-4614-7803-4